Effects of hydrogen dilution and B-doping on the density of Si–C bonds and properties of *a*-Si_xC_{1-x}:H films

J. Herrera-Celis*, C. Reyes-Betanzo, A. Itzmoyotl- Toxqui
Instituto Nacional de Astrofísica, Óptica y Electrónica (INAOE)
Luis Enrique Erro #1, Santa María Tonantzintla, San Andrés Cholula 72840, Puebla, México

A. Orduña-Diaz
Centro de Investigación en Biotecnología Aplicada del Instituto Politécnico Nacional (CIBA-IPN)
Ex-Hacienda San Juan Molino, Carr. Estatal Tecuexcomac-Tepetitla Km 1.5, Tepetitla 90700, Tlaxcala, México
(Received: September 25th, 2015; Accepted: April 19th, 2016)

This work presents a study on the effects of hydrogen dilution and boron doping on the formation of Si–C and Si–H bonds during the deposition of hydrogenated amorphous silicon carbon alloy films by plasma-enhanced chemical vapor deposition. Low power densities of 25 mW/cm^2 and 50 mW/cm^2, high pressure of 1.5 Torr, temperatures of 150 °C and 200 °C, and methane-silane gas flow ratios of 0.70 and 0.85 were chosen in order to obtain suitable films for biomedical and biological applications. FTIR spectroscopy, UV-Vis spectroscopy, atomic force microscopy and electrical dark conductivity measurements were carried out to characterize the films. The results show that hydrogen dilution decreases CH_n groups in the films and increases the Si–C and Si–H bond densities, whereas B-doping decreases the Si–C and Si–H bond densities. Undoped films with optical band gap of 2.47 eV and conductivity around of 5×10^{-10} S/cm, and B-doped films with a root mean square roughness of about 1 nm and a conductivity of the order of 10^{-6} S/cm were obtained.

Keywords: plasma-enhanced chemical vapor deposition; hydrogenated amorphous silicon carbon alloy; material properties

Introduction

Although the requirements of a material for biomedical applications as coatings for implants [1] or implantable devices [2] are different of those for biological applications as cell culturing [3], tissue regeneration [4] and biosensors [5], there are two properties in common: biocompatibility and no cytotoxicity. A biocompatible material must be chemically stable and must have low dissolution rate in biological medium to avoid any adverse reactions, whereas a no cytotoxic material is not toxic to cells [6]. Undoubtedly, the development of these properties by a material is closely related to the elements that are part of the material and the chemical bonds between them, which result in the material structure. Materials to be included into devices must be obtained under compatible conditions with the fabrication processes of the devices. Furthermore, the properties of the materials must be in accordance with its specific role into devices [7]. For all these reasons, the success of a material in an application depends on the correct definition of the mechanism and the parameters to obtain it.

According to previous published works [8], hydrogenated amorphous silicon carbon alloy (*a*-Si_xC_{1-x}:H) is a candidate for biomedical and biological applications, among other reasons because its chemical structure is based in chemical bonds of silicon, carbon and hydrogen. In this work plasma-enhanced chemical vapor deposition (PECVD) is used to obtain *a*-Si_xC_{1-x}:H films with a narrow range of deposition parameters considering these applications. Furthermore, a study on the influence of methane-silane gas flow ratio (X_{CH4}), hydrogen dilution and doping level on the morphology, the formation of Si–C bonds, and the optical and electrical properties of the films is addressed.

Experimental

The deposition processes of *a*-Si_xC_{1-x}:H films were carried out in a ultra-high-vacuum multi-chamber PECVD system (*MVSystem Inc.*), which operates at a radio frequency of 13.56 MHz. All *a*-Si_xC_{1-x}:H films were deposited with precursor gases of silane (SiH_4) diluted at 10% in H_2 and methane (CH_4), onto 2947 Corning glasses, p-type silicon substrate (100), and titanium stripes on glasses. Hydrogen (H_2) was used as a carrier and diluent gas. Taking into account that the compatibility of the deposition process with the Si-based microfabrication technology and the applications increases when low deposition temperatures are used [2, 7], temperatures of 150 °C and 200 °C were selected. To obtain carbon-rich films, methane-silane gas flow ratios (X_{CH4}) of 0.70 and 0.85 were chosen. According to Iliescu *et al*. [3], under high pressures the films obtained have good uniformity, then the pressure was set to 1.5 Torr. Under low deposition power density, the deposition process is controlled by the reaction of silane radicals with methane molecules, making the deposition more orderly [9]. Two power densities of 25 mW/cm^2 and 50 mW/cm^2 were defined to achieve this effect.

Two hydrogen dilution (Z_{H2}) of 2.7 and 9 were set to study its influence in the material properties. Finally, some films were doped from 0.5% to 2.5% using diborane (B_2H_6) as dopant gas (B-doped *a*-Si_xC_{1-x}:H films). All the deposition processes are shown in Table 1.

* jlhc@inaoep.mx

Table 1. Deposition parameters of the PECVD processes, and deposition rate, root-mean square roughness (Rq), density of Si–C bonds (N_{SiC}), density of C–H bonds (N_{CH}) and density of Si–H bonds (N_{SiH}) of undoped and B-doped *a*-Si_xC_{1-x}:H films.

PECVD process	X_{CH4}	Z_{H2}	Y_B (%)	Power density (mW/cm^2)	T (°C)	Deposition rate (nm/min)	R_q (nm)	N_{SiC} (bond/cm^3)	N_{CH} (bond/cm^3)	N_{SiH} (bond/cm^3)
aSiC-01	0.7	2.7	0	50	150	11.17 ± 0.16	2.33 ± 0.34	2.09×10^{21}	1.16×10^{22}	4.69×10^{21}
aSiC-02	0.7	9.0	0	50	150	7.65 ± 0.05	1.00 ± 0.09	1.54×10^{21}	1.60×10^{22}	4.08×10^{21}
aSiC-03	0.85	2.7	0	50	150	11.95 ± 0.12	0.88 ± 0.02	1.10×10^{21}	1.34×10^{23}	2.96×10^{21}
aSiC-04	0.85	9.0	0	50	150	6.29 ± 0.01	0.88 ± 0.21	1.78×10^{21}	1.67×10^{22}	3.08×10^{21}
aSiC-05	0.7	2.7	0	50	200	11.67 ± 0.17	1.11 ± 0.16	2.10×10^{21}	1.38×10^{22}	3.87×10^{21}
aSiC-06	0.7	9.0	0	50	200	7.95 ± 0.11	0.96 ± 0.06	2.27×10^{21}	2.25×10^{22}	4.11×10^{21}
aSiC-07	0.85	2.7	0	50	200	11.32 ± 0.11	1.20 ± 0.12	3.02×10^{21}	6.34×10^{22}	3.29×10^{21}
aSiC-08	0.85	9.0	0	50	200	6.43 ± 0.10	1.00 ± 0.16	3.16×10^{21}	3.49×10^{22}	3.62×10^{21}
aSiC-09	0.85	2.7	0	25	200	7.35 ± 0.07	0.50 ± 0.04	1.74×10^{21}	9.90×10^{22}	3.38×10^{21}
aSiC-10	0.85	9.0	0	25	200	6.55 ± 0.04	0.70 ± 0.07	4.24×10^{21}	3.54×10^{22}	3.95×10^{21}
aSiC-11	0.85	9.0	0.5	25	200	6.04 ± 0.07	0.60 ± 0.07	3.47×10^{21}	2.67×10^{22}	2.94×10^{21}
aSiC-12	0.85	9.0	1.0	25	200	7.88 ± 0.14	0.96 ± 0.03	4.69×10^{21}	3.80×10^{22}	2.69×10^{21}
aSiC-13	0.85	9.0	2.0	25	200	6.90 ± 0.04	0.97 ± 0.05	3.21×10^{21}	2.76×10^{21}	2.35×10^{21}
aSiC-14	0.85	9.0	2.5	25	200	8.11 ± 0.13	1.14 ± 0.05	2.30×10^{21}	4.77×10^{22}	1.91×10^{21}

Measurements and results

Deposition rate and surface morphology

Thicknesses of the films were measured in a surface profiler *KLA Tenkor P-7*, while their surface morphologies were measured in an AFM *Nanosurf easyScan DFM*. The quantitative results are listed in the Table 1. According to these results, the hydrogen dilution affects significantly the deposition rate, almost duplicating its value in some cases, going from 6.30 to 11.95 nm/min. A similar effect is appreciated when the X_{CH4} is decreased, but in this case the change occurs in much lower proportion. In contrast, the roughness is mainly affected by the power density of deposition. At power density of 25 mW/cm^2 all the films have a root-mean square roughness less to 1 nm, except the aSiC-14 process, whose roughness is affected by the doping level. None temperature tendency is evident in these results.

Structural and vibrational characterization

The structural properties of the *a*-Si_xC_{1-x}:H films were studied using a FTIR spectrometer *Bruker Vector 22*, operating in absorbance mode in middle infrared (500 – 3500 cm^{-1}). The absorption spectra were normalized by the corresponding thicknesses and the assignment of peaks in the spectra are listed in Table 2. According to the results in Figure 1, the peaks at 1000 cm^{-1}, 1245 cm^{-1} and inside the band from 2860 to 2960 cm^{-1} decreases, while the peak in the band from 630 to 650 cm^{-1} increases, when Z_{H2} goes from 2.7 to 9. Furthermore, the peak in the band from 740 to 800 cm^{-1} becomes more pronounced than the peak at 640 cm^{-1} when the X_{CH4} goes from 0.70 to 0.85. From the viewpoint of bonding, significant changes are not observed about power density (see also Figure 2). These statements may be corroborated based on densities of Si–C, Si–H and C–H bonds (N_{SiC}, N_{SiH} and N_{CH}) presented in Table 1, which were calculated following the procedure used in [13].

The FTIR spectrum of the film corresponding to the aSiC-14 process in Figure 2 includes two peaks at 975 and 1150 cm^{-1}, which are assigned to the wagging and bending vibration modes of B–H bonds, respectively [14]. In the other spectra of the B-doped films only one shoulder at the left of the peak at 1000 cm^{-1} is observed, while no peak at 1150 cm^{-1} is displayed. The peaks in the band 2350 – 2650 cm^{-1} corresponding to B–H_n bonds do not appear [15].

Optical characterization

The UV-visible spectroscopy was carried out in a spectrophotometer *Perkin Elmer Lambda 3* from 190 to 900 nm, in order to obtain some optical properties of the films and correlate them with deposition parameters. Using the transmittance spectra and the Tauc equation given by [16]:

$$(\alpha h\nu)^{1/2} = B(h\nu - E_{gopt}), \quad (1)$$

where h is the Planck's constant and ν is the radiation frequency, the optical band gap (E_{gopt}) and the Tauc parameter (B factor) were found. B factor is a parameter that indicates the amount of disorder in a film [17].

The data fitting procedure using (1) resulted in the values summarized in Table 3. E_{gopt} decreases around of 0.16 eV and 0.24 eV for X_{CH4} of 0.7 and 0.85, respectively, when Z_{H2} changes from 2.7 to 9.0. In undoped films, a trend is observed in B factor versus temperature under the same other deposition parameters, its value is higher at 200 °C than at 150 °C in the majority of cases. Regarding other deposition

Table 2. Assignment of bonds and vibrational modes of the absorption peaks in the infrared spectra of undoped *a*-Si_xC_{1-x}: H films.

Assignment	Wavenumber (cm^{-1})	References
Si–H_n wagging	630–650	[10, 11]
Si–C stretching, Si–CH_n wagging	740–800	[2, 10–13]
Si–H_2 rocking, scissors	845, 895	[11]
CH_n wagging, Si-CH_3 bending	1000, 1245	[10, 11, 13]
C–CH_3, CH_n bending and scissors	1370, 1450	[11]
C=C stretching	1540, 1630	[11, 12]
Si–H_2 stretching	2080	[10–13]
CH_n sp^3 stretching	2860–2960	[10–13]

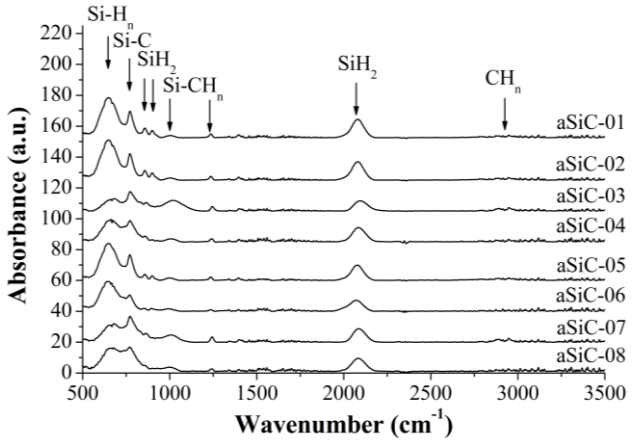

Figure 1. FTIR spectra of undoped *a*-Si_xC_{1-x}:H films.

parameters (X_{CH4}, Z_{H2} and power density), according to the results, their effect on *B* factor depends of the state of the remaining parameters. In B-doped films, the doping level decreases both E_{gopt} and *B* factor.

Electrical characterization

Electrical dark conductivity measurements were carried out in the range of 300 – 440 K with a step of 10 K within the chamber of a *Janis Research* cryostat maintaining a pressure of 70 mTorr. Current–voltage measurements were made by using a *Keithley 6517A* and a *LakeShore 331* temperature controller. Before measurements, the structures of undoped and B-doped *a*-Si_xC_{1-x}:H/titanium on glass were annealed at 140 °C in nitrogen atmosphere for 2 hours to improve the contact between the material and titanium. In the Figure 3 can be seen that the curves are shifted upward by the change in hydrogen dilution from 2.7 to 9.0. This effect is more apparent in the films deposited at X_{CH4} = 0.85 than X_{CH4} = 0.70. In contrast, the B-doping not only shifts upward the curve but also changes its slope.

The values of conductivity for undoped and B-doped films calculated using the current–voltage measurements fall on

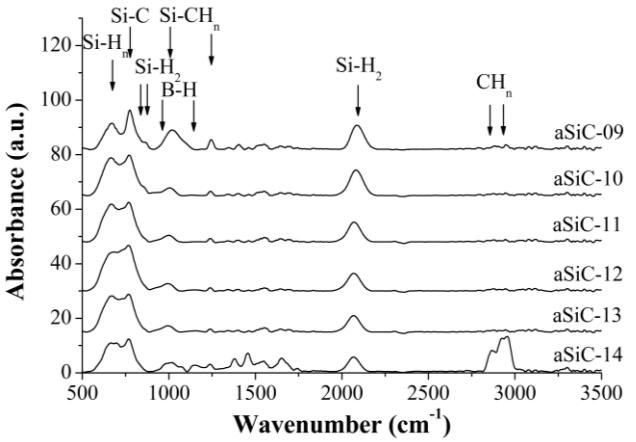

Figure 2. FTIR spectra of undoped (Y_B = 0.0%) and B-doped *a*-Si_xC_{1-x}:H films.

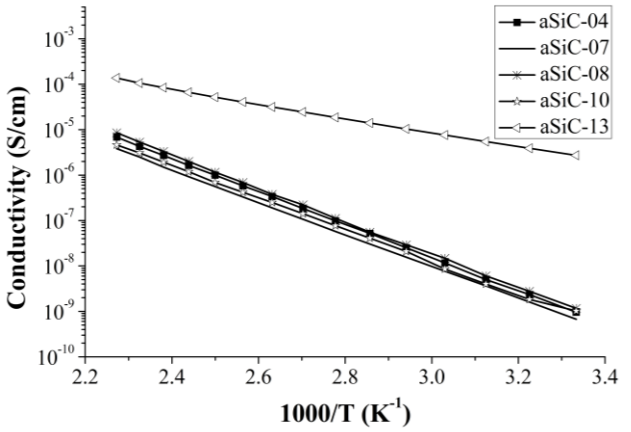

Figure 3. Temperature dependence of the dark-conductivity of undoped and B-doped *a*-Si_xC_{1-x}:H films.

one straight line; this straight line represents a thermally activated conduction regime and can be described by the following equation [18]:

$$\sigma_D = \sigma_0 \exp(-E_\sigma/k_BT), \quad (2)$$

where σ_D is the dark electrical conductivity, σ_0 is the prefactor, E_σ is the activation energy, k_B is the Boltzmann constant, and *T* is the temperature. The Table 3 shows the results obtained by fitting the measurement data to (2). The results of this procedure show minor changes in E_σ and major changes in σ_0 by changes in hydrogen dilution, and major changes in E_σ and minor changes in σ_0 by B-doping.

Discussion

a-Si_xC_{1-x}:H as material for interaction with biological media is one of the applications in which this material is suitable [1, 2]. Its success in this applications (e.g. implants and implantable devices) is related with its density of Si–C bonds, its density of states (DOS) inside the band gap and its conductivity [8, 19]. N_{SiC} enhances the biocompatibility, inasmuch as Si–C bond (301 kJ/mol) is stronger than Si–Si bond (226 kJ/mol) [20], which results in greater chemical

Table 3. Optical band gap (E_{gopt}), Tauc parameter (B), activation energies (E_σ), prefactor (σ_0) and conductivity at 300 K (σ_{rt}) of undoped and B-doped a-Si_xC_{1-x}:H films.

PECVD process	Z_{H2}	T (°C)	E_{gopt} (eV)	B $(eV\,cm)^{-1/2}$	E_σ (eV)	σ_0 (S/cm)	σ_{rt} (S/cm)
Undoped a-Si_xC_{1-x}:H films: X_{CH4} = 0.7, 50 mW/cm²							
aSiC-01	2.7	150	2.05	497.75	0.73	954.90	1.05×10^{-9}
aSiC-02	9.0	150	1.90	489.34	0.73	1225.10	1.47×10^{-9}
aSiC-05	2.7	200	2.01	514.58	0.67	205.35	3.98×10^{-9}
aSiC-06	9.0	200	1.84	498.28	0.73	1166.05	1.08×10^{-9}
Undoped a-Si_xC_{1-x}:H films: X_{CH4} = 0.85, 50 mW/cm²							
aSiC-03	2.7	150	2.47	426.24	0.70	369.57	5.55×10^{-10}
aSiC-04	9.0	150	2.23	523.64	0.74	2024.49	9.57×10^{-10}
aSiC-07	2.7	200	2.43	466.99	0.73	975.36	6.71×10^{-10}
aSiC-08	9.0	200	2.19	513.39	0.75	3757.39	1.17×10^{-9}
Undoped a-Si_xC_{1-x}:H films: X_{CH4} = 0.85, 25 mW/cm²							
aSiC-09	2.7	200	2.42	534.74	--	--	--
aSiC-10	9.0	200	2.17	491.02	0.71	573.36	1.02×10^{-9}

PECVD process	Y_B (%)	E_{gopt} (eV)	B $(eV\,cm)^{-1/2}$	E_σ (eV)	σ_0 (S/cm)	σ_{rt} (S/cm)
B-doped a-Si_xC_{1-x}:H films: X_{CH4} = 0.85, Z_{H2} = 9.0, 25 mW/cm², 200 °C						
aSiC-11	0.5	1.96	449.68	0.41	0.81	1.72×10^{-7}
aSiC-12	1.0	1.81	385.99	0.35	0.29	3.95×10^{-7}
aSiC-13	2.0	1.80	395.70	0.33	0.73	2.72×10^{-6}
aSiC-14	2.5	1.77	379.61	0.33	0.35	1.26×10^{-6}

stability and low dissolution [6].

The Figure 2 shows that the peak at 780 cm^{-1} is affected by both X_{CH4} and Z_{H2}. Increasing X_{CH4} from 0.70 to 0.85, N_{SiC} increases and N_{SiH} decreases because there are more methane molecules per radical silane; increasing Z_{H2} from 2.7 to 9.0, N_{SiC} and N_{SiH} increase. Hydrogen completes the dangling bonds in the amorphous structure, reducing the DOS within the band gap and improving the conductivity [21]. But in this case, under low power density of deposition, that is not the only effect. Considering the disappearance of the peaks in the band 2800 – 3000 cm^{-1} of the absorption spectra when hydrogen dilution is increased, hydrogen removes methyl groups, promoting the formation of Si–C and Si–H bonds and avoiding soft graphite-like structure.

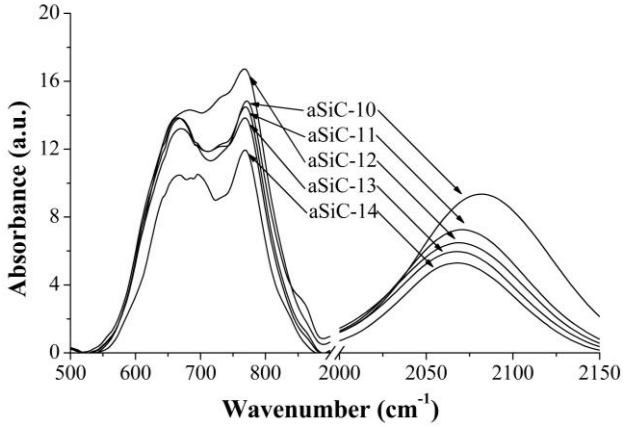

Figure 4. FTIR spectra in the ranges 500–900 cm^{-1} and 2000 – 2150 cm^{-1} of undoped and B-doped a-Si_xC_{1-x}:H films.

Different trend is observed with doping. The Figure 4 shows that the peaks close to 770 cm^{-1} and 2080 cm^{-1} are reduced as the B-doping level increases (except the spectrum of the film corresponding to the aSiC-12 process), which means that B-doping decreases N_{SiC} and N_{SiH} (see also Table 1). In this case, the absorption by CH_n groups increases as the doping level increases, achieving in the sample doped at 2.5% similar levels of absorption to those of Si–C bonds. This shows that as the doping level increases, the deposition control by reaction of methane and diborane molecules with silicon radicals is lower (dynamics of deposition). It increases both disorder within the amorphous structure and the surface roughness of the films. Furthermore, the peak at 2080 cm^{-1} shifts to 2060 cm^{-1} as the doping level increases. It is probable that this is due to lower concentration of carbon atoms and to the presence of boron atoms.

Returning to the results of the optical and electrical characterizations, the ranges of E_{gopt}, B factor, E_σ and σ_o of undoped films are 1.84 – 2.47 eV, 426 – 534 $(eV\,cm)^{-1/2}$, 0.67 – 0.75 eV and 205–3757 S/cm, respectively. According

to this results, it is possible to modulate the E_{gopt} in 0.63 eV changing X_{CH4} from 0.70 to 0.85 and Z_{H2} from 2.7 to 9.0 without affect the band tails drastically; furthermore, the conductivity can be improved by passivation of dangling bonds increasing Z_{H2}. In contrast, the doping, even though increases the conductivity in three orders of magnitude (from 1.02×10^{-9} to 2.72×10^{-6} S/cm at room temperature), also decreases E_{gopt} to 1.77 eV and increases the disorder, due to the minor content of carbon and to different bond lengths of the bonds formed by boron, respectively.

Applications as biosensors require a process known as bio-functionalization. This process is easier to achieve in smooth surfaces than in rough surfaces [22]. This work, consequently with other study [19], found that the deposition parameter that most affect the surface morphology is the power density. Films deposited at 25 mW/cm^2 have root-mean square roughness less than or equal to 1 nm, even in B-doped films, where the incorporation of boron increases the disorder and the surface roughness. Again, these results are explained from the dynamics of deposition.

Other type of applications as neural interface devices [2], unlike these mentioned before, require a biocompatible material to encapsulate the device. In this case the deposition temperature must be lower than 200 °C and the conductivity must be as low as possible. Taking into account the requirements, the aSiC-03 process is the most optioned to fulfill this task. This process is carried out at 150 °C and a conductivity of 5.55×10^{-10} S/cm at room temperature was achieved in the corresponding film.

Summary and conclusions

By means of this study, the effects of hydrogen dilution and B-doping on the surface morphology and the structural, optical and electrical properties of *a*-Si_xC_{1-x}:H films obtained by PECVD have been assessed under low power density, high pressure and low temperature deposition. The combination of high pressure and low power density allows to obtain root-mean square roughness in the sub-nanometric scale even in B-doped films, which is important when a bio-functionalization process is required to use the material. According to the results, hydrogen and diborane molecules compete with methane molecules and silane radicals to incorporate into the film by reaction with other silane radicals. Consequently, the methane-silane gas flow ratio must be kept high to prevent that the density of Si–C bonds is decreased and with it the biocompatibility of the material is impaired as well. The hydrogen dilution and B-dopind level must be low whether high optical band gap and low conductivity are required. In contrast, high hydrogen dilution, high B-doping level and high methane-silane gas flow ratio must be set to achieve high Si–C bond density, low DOS inside band gap and high conductivity regardless of the low optical band gap and the broader band tails.

Acknowledgment

This work was supported by the National Council of Science and Technology (CONACyT) under the project No. 242440.

References

[1]. S. Cogan. D. Edell. A. Guzelian, Y. Liu, E. Edell, *J. Biomed. Mater. Res. A* **67**, 856 (2003).
[2]. J. Hsu, P. Tathireddy, L. Rieth, A. Normann, F. Solzbacher, *Thin Solid Films* **516**, 34 (2007).
[3]. C. Iliescu, B. Chen, D. Poenar, Y. Lee, *Sens. Actuators B Chem.* **129**, 404 (2007).
[4]. O. Palyvoda, C. Chen, G. Auner, *Biosens. Bioelectron.* **22**, 2346 (2007).
[5]. E. Galopin, L. Touahir, J. Niedziołka-Jönsson, R. Boukherroub, A. Gouget-Laemmel, J. Chazalviel, F. Ozanam, S. Szunerits, *Biosens. Bioelectron.* **25**, 1199 (2010).
[6]. S.E. Saddow, *Silicon Carbide Biotechnology*, 1st ed. (Elsevier, 2012).
[7]. C. Iliescu, D.P. Poenar, in: *Physics and Technology of Silicon Carbide Devices*, Ed. Y. Hijikata (InTech, 2013) p. 131-134.
[8]. M. Fraga, R. Pessoa, M. Massi, H. Maciel, in: *Physics and Technology of Silicon Carbide Devices*, Ed. Y. Hijikata (InTech, 2013) p. 313-336.
[9]. I. Pereyra, M. Carreño, M. Tabacniks, R. Prado, M. Fantini, *J. Appl. Phys.* **84**, 2371 (1998).
[10]. E. Chen, G. Du, Y. Zhang, X. Qin, H. Lai, W. Shi, *Ceram. Int.* **40**, 9791 (2014).
[11]. V. Tolstoy, I. Chernyshova, V. Kkryshevsky, *Handbook of infrared spectroscopy of ultrathin films*, 1st ed. (John Wiley & Sons, 2003).
[12]. W.K. Choi, S. Gangadharan, *Mat. Sci. Eng. B* **75**, 174 (2000).
[13]. M.M. Kamble, V.S. Waman, A.H. Mayabadi, S.S. Ghosh, B.B. Gabhale, S.R. Rondiya, A.V. Rokade, S.S. Khadtare, V.G. Sathe, T. Shripathi, H.M. Pathan, S.W. Gosavi, S.R. Jadkar, *J. Coatings* **2014**, 905903 (2014).
[14]. B. Stuart, *Infrared spectroscopy: fundamentals and applications*, 1st ed. (John Wiley & Sons, 2004).
[15]. S. Shen, M. Cardona, *J. Phys. Colloq.* **42**, 349 (1981).
[16]. J. Tauc, R. Grigorocivi, A. Vancu, *Phys. Status Solidi* **15**, 627 (1966).
[17]. D. Sala, P. Fiorini, A. Frova, A. Gregori, A. Skumanich, N.M. Amer, *J. Non-Crist. Solids* **77/78**, 853 (1985).
[18]. K. Tanaka, E. Maruyama, T. Shimada, H. Okamoto, *Amorphous Silicon*, 1st ed. (Wiley, 1999) p. 136-137.
[19]. J. Herrera-Celis, C. Reyes-Betanzo, A. Itzmoyotl-Toxqui, A. Orduña-Díaz, A. Perez-Coyotl, *J. Vac. Sci. Technol. A* **33**, 1 (2015).
[20]. J. Bullot, M. Schmidt, *Phys. Stat. Sol. B* **143**, 345 (1987).
[21]. K. Tanaka, E. Maruyama, T. Shimada, H. Okamoto, *Amorphous Silicon*, 1st ed. (Wiley, 1999) p. 111-118.
[22]. T. Tätte, K. Saal, I. Kink, A. Kurg, R. Lohmus, U. Mäeorg, M. Rahi, A. Rinken, A. Lohmus, *Surf. Sci.* **532**, 1085 (2003).